MASTER

TITLE: MATERIALS ANALYSIS WITH A NUCLEAR MICROPROBE

AUTHOR(S): Carl J. Maggiore

los alamos
scientific laboratory
of the University of California
LOS ALAMOS, NEW MEXICO 87545

An Affirmative Action/Equal Opportunity Employer

MATERIALS ANALYSIS WITH A NUCLEAR MICROPROBE

by

Carl J. Maggiore
University of California
Los Alamos Scientific Laboratory
Los Alamos, NM 87545

E-DO-011-80 ED0080.HA

MATERIALS ANALYSIS WITH A NUCLEAR MICROPROBE

by

Carl J. Maggiore
University of California
Los Alamos Scientific Laboratory
Los Alamos, NM 87545

ABSTRACT

The ability to produce focused beams of a few MeV light ions from Van de Graaff accelerators has resulted in the development of nuclear microprobes. Rutherford backscattering, nuclear reactions, and particle-induced x-ray emission are used to provide spatially resolved information from the near surface region of materials. Rutherford backscattering provides nondestructive depth and mass resolution. Nuclear reactions are sensitive to light elements $(Z < 15)$. Particle-induced x-ray analysis is similar to electron microprobe analysis, but 2 orders of magnitude more sensitive. The focused beams are usually produced with specially designed multiplets of magnetic quadrupoles. The LASL microprobe uses a superconducting solenoid as a final lens. The data are acquired by a computer interfaced to the experiment with CAMAC. The characteristics of the information acquired with a nuclear microprobe are discussed; the means of producing the beams of nuclear particles are described; and the limitations and applications of such systems are given.

I. INTRODUCTION

There are several well-known analytical techniques for obtaining spatially resolved information from materials. These include electron microprobe analysis, scanning auger microanalysis, ion microprobe analysis, laser microprobe, and scanning electron microscopy using various analytical signals. But surface analytical problems are often of sufficient complexity that an experimenter needs more than one technique to resolve ambiguities. Pecent developments in the production and use of focused beams of 0.5 to 5.0 MeV light ions have resulted in a "new" analytical instrument, the nuclear microprobe. This tool will not solve all problems but is complementary to existing techniques.[1] The purpose of this paper is to review the various analytical signals obtained with beams of nuclear particles and the means of producing microbeams of such particles.

II. ANALYTICAL SIGNALS

When a beam of few million electron volts light ions (protons, deuterons, tritons, ^{3}He, or alpha particles) strikes the surface of a specimen, several things can happen. Figure 1 shows schematically some of the possibilities. The multiplicity of results is due to the relatively high energy of the incident beam. The three signals of primary interest for a nuclear microprobe are (1) elastically backscattered particles, (2) nuclear reaction products and γ rays, and (3) characteristic x rays. Since the use of backscattered particles and nuclear reaction products may not be familiar to most people in the SEM community, a brief review of the information obtained by these methods will be given.

A. Rutherford Backscattering (RBS)

The concentration vs depth of an element in the near surface region of a solid can be determined nondestructively by measuring the energy of the incident particles elastically scattered from the nuclei in the solid.[2,3] Figure 2 shows schematically a typical backscattering experiment and notation. Throughout this discussion it will be assumed that M_1, the mass of the incident particle, is less than M_2, the mass of the target nucleus. If there is no nuclear reaction, simple conservation of energy and momentum can be used to calculate the energy of the backscattered particle. Let the kinematic factor, $K = E'/E$, that is, the ratio of the energy of the incident particle to the energy of

the particle after scattering,

$$K = \frac{E'}{E} = \left[\frac{M_1 \cos\theta + \sqrt{M_2^2 - M_1^2 \sin^2\theta}}{M_1 + M_2} \right]^2 . \quad (1)$$

From Eq. (1), it can be seen that a knowledge of the incident and scattered energy enables one to calculate the mass M_2 of the target nucleus. Mass analysis of the target is obtained by kinematic constraints, conservation of energy and momentum.

Depth analysis is possible because the incident particle loses energy in a known way as it enters the specimen before backscattering and as it leaves the specimen. By measuring the total energy loss of the particle entering and leaving the specimen, the depth at which the collision occurred can be deter-mined. The incident particle loses energy primarily by ionization and excitation of electrons in the sample. This energy loss is the source of the characteristic x-ray signal to be discussed later.

Figure 3 shows the backscattering spectrum obtained from a thin, high-Z film on a low-Z substrate. The broad high-energy peak is due to scattering in the film; it is kinematically separated from the lower energy backscattering from the lower mass substrate. The high-energy limit KE_{in} is due to scattering from the front surface of the thin film. The low-energy limit E_f is due to scattering from the back surface of the film. The energies between KE_{in} and E_f are due to scattering from successively deeper layers within the film. The asymmetry in the peak is due to the change in scattering cross section as a function of energy.

The energy loss of a particle per unit path length is not a constant but depends on the energy of the projectile and charge and mass of both the target and incident particle. At high energies (>10 MeV/amu), the energy loss process is well understood theoretically by the Bethe-Bloch formalism. This is not the case at lower energies, and one resorts to compilations of experimental data for specific projectile, target, and energy.[4,5,6]

For backscattering analysis, the energy loss is usually expressed in terms of the stopping power, $S(E) = dE/Ndx = eV/10^{15}$ atoms/cm^2 where N is the atomic density. Figure 4 shows the stopping power for alpha particles in gold and is typical of stopping power curves in general. The data are from actual measurements, and the solid curve is the result of Ziegler's fit to the available literature.[6,7] The energy loss is given in terms of Ndx, the number of atoms/cm^2, rather than actual depth because it does not depend on the density of the film, which may differ from that of bulk material. Furthermore, Bragg's Rule for the addition of stopping powers of compounds applies at the atomic level.[8,9,10]

Using the geometry of Fig. 3, the thickness of the film can be calculated in the following manner. The energy of the incident beam before scattering from the back surface of the film is

$$E_t = E_{in} - \int_0^{t/\cos\theta} {}^{in} \frac{dE}{dx} dx \quad .$$

(2)

The particle loses energy in the collision and continues to lose energy as it leaves the specimen, so the final detected energy is

$$E_f = KE_t - \int_0^{t/\cos\theta} {}^{out} \frac{dE}{dx} dx \quad .$$

(3)

Letting $E = KE_{in} - E_f$ and substituting Eq. (2) in Eq. (3), we have

$$E = \int_0^{t/\cos\theta} {}^{in} \frac{dE}{dx} dx - \int_0^{t/\cos\theta} {}^{out} \frac{dE}{dx} dx \quad .$$

(4)

This integral equation relates the measured energy loss E to the unknown thickness t. There are numerous approximations that can be made to simplify Eq. (4) depending on the thickness of the film.[2,3] It is not appropriate to

discuss these approximations in more detail here but merely to note that the absolute depth of a target atom is obtained nondestructively, that is, without ion milling or altering the specimen. The formalism outlined above applies not only to thin films on the surface but is generally applicable to any target atom at a measurable depth beneath the surface.

Ernst Rutherford solved the problem of coulomb scattering of an ion from a target nucleus in 1911.[11] The differential cross section for scattering is written as

$$\frac{d\sigma}{d\Omega} = \left(\frac{Z_1 Z_2 e^2}{4E}\right)^2 \frac{4}{\sin^4\theta} \frac{\left\{\cos\theta + \left[1 - \left(\frac{M_1}{M_2}\sin\theta\right)^2\right]^{1/2}\right\}^2}{\left[1 - \left(\frac{M_1}{M_2}\sin\theta\right)^2\right]^{1/2}} \quad , \qquad (5)$$

where Z_1 and Z_2 are the atomic numbers of the incident and target nuclei. θ is the laboratory scattering angle in Fig. 2, e is the charge on an electron, and E is the energy of the incident particle before scattering. The total average scattering section is

$$\sigma = \frac{1}{\Omega}\int \frac{d\sigma}{d\Omega} \, d\Omega \quad , \qquad (6)$$

where the integral is over the solid angle Ω of the detector. It is proportional to the probability of scattering of the incident projectile into the detector from the target nucleus. It enables one to make quantitative analyses using Rutherford backscattering. Figure 5 shows the effective scattering cross section in counts, $A = Q\sigma\Omega$ Nt, for 1 MeV alpha particles from target nuclei at a back angle of 160°.[10] Since the coulomb scattering cross section can be calculated exactly, quantitative analysis is possible without standards of similar composition.

Backscattering spectrometry has been used for a wide variety of problems and excellent reviews of the literature have been made.[3,12,13] The applications usually fall into one of the following classes: (1) thin film studies, (2) surface contamination, (3) ion implantation depth and concentration, (4) bulk sample doping level, and (5) compound target studies involving changing

composition with depth. In general the technique is well suited to problems involving the detection of heavy elements in the presence of a light substrate. Depth resolution of 20 nm in the outer micron of a sample is routinely possible. Better depth resolution is possible by using grazing incidence or exit angles.

The technique is not well suited to depth measurements at large depths ($>10~\mu$m) because of energy straggling and the inherent ambiguity between depth and mass resolution. Furthermore, the mass resolution is not particularly good for higher Z materials. Figure 6 shows the kinematic factor K for alpha particles vs Z of the target. The Z^2 dependence of the cross section in Eq. (5) and the lower energy of backscattered particles means that backscattering is not sensitive for light elements on a heavy substrate.

Until the advent of nuclear microprobes, the sample had to be uniform over the dimensions of the beam (1 - 2 mm diameter). The nondestructive depth resolving ability of backscattering in conjunction with spatially resolved beams means that three-dimensional microscopy of bulk samples in the near surface region is now possible.

B. Nuclear Reactions

The main limitation of Rutherford backscattering is that it is not sensitive to low Z elements because of the high background from the substrate and the low cross section for elastic scattering. Nuclear reaction techniques offer highly selective methods of probing the near surface region of materials for light elements.[14,15,16] The method is based on the fact that a nuclear reaction can occur if the incident particle has sufficient energy to overcome the coulomb barrier of the target nucleus. The electrostatic potential energy scales as $Z_1 Z_2/r$ with r equal to the separation between the target and projectile nuclei. For the light incident ions and energies less than 5 MeV, this means the nuclear reaction technique can be used for $Z_2 < 15$.

In general a nuclear reaction is written as A(B,C)D where

$$A + B \rightarrow C + D + Q \quad . \tag{7}$$

A is the target nucleus; B is the incident projectile; C is the reaction pro-

- 7 -

duct; D is the residual nucleus; and Q is energy released in the reaction. For Rutherford backscattering, A = D, B = C, Q = 0, and the interaction occurs by the electrostatic force only. For a nuclear reaction, much more flexibility is allowed because the interaction occurs by way of the nuclear foｒce. Particles may be absorbed or emitted from the nucleus, and the residual nucleus may be left in its ground state or an excited state.

The reactions of most interest for light element analysis are those in which the reaction product is easily detected, free from interferences, and has a large cross section. Silicon surface barrier detectors are usually used to detect charged particles, and germanium or NaI(Tl) counters are used to detect gamma rays. Reactions with positive Q values such as (d,p), (p,α), (d,α), or (p,γ) are often used. Table I lists some of the most commonly used nuclear reactions for light element detection.[12]

There are several characteristics of nuclear reactions that add to the complexity of the data analysis but also make them specific and useful. Notice in Table I that the reactions are isotope dependent; for example, there is a useful (p,α) reaction for ^{18}O and a (d,p) reaction for ^{16}O. This means that one can use isotopically enriched samples or processing to monitor migration of atoms in the specimen.

For the (d,p) reaction on ^{16}O, there is the ground state reaction $^{16}O(d,p_0)^{17}O$ with a Q value of 1.92 MeV and the reaction to the first excited state $^{16}O(d,p_1)^{17}O$ with a Q value of 1.05 MeV. Figure 7 shows schematically what happens in the reactions.[17] Protons with two different energies would be observed experimentally. The multiple peaks in the spectrum can be used to resolve ambiguities when contaminant peaks are present.

At the low incident energies used for materials analysis, the cross section for a given reaction may change rapidly vs energy. Figure 8 shows a typical cross section schematically. Variations of a factor of 10 over energy ranges of a few hundred kiloelectron volts are not unusual. This means the sensitivity of the proving incident beam is not a constant, but may change rapidly with depth because energy of the beam is decreasing as it enters the specimen. A depth distribution for a thick target could be obtained by deconvolution if needed; it would be straightforward but nontrivial for differing charged particles entering and leaving the specimen. For a (p,γ) reaction, the problem is much easier

- 8 -

since there is little absorption of the gamma rays in the target; the resonances are narrower; and successively deeper layers of the specimen may be sampled by increasing the energy of the beam. The technique is not, however, compatible with microprobe work because it involves changing the energy of the accelerator.

C. Particle-Induced X-ray Emission (PIXE)

The use of electron-beam-induced x rays is well known in the SEM community. PIXE can be used in the same way to obtain spatially resolved elemental maps with the nuclear microprobe. There are excellent reviews of the PIXE technique and its applications in the literature.[19-22]   Since the techniques are so similar and well known, no general discussion of the method will be given here. However, it is appropriate to explain the reasons for the increased sensitivity obtained with a nuclear microprobe.

The lower detectable limit of any x-ray analysis is determined by the background radiation under the characteristic peaks. The continuous bremsstrahlung is a fundamental limitation because it is inherently associated with the slowing down of the charged particles in the incident beam. There are four main sources of background radiation observed in an x-ray spectrum obtained with a Si(Li) detector: (1) bremsstrahlung from the projectile, (2) bremsstrahlung from "knock on" electrons or delta rays, (3) Compton scattering of x rays from nuclear excitations, (4) tailing in the detector itself due to incomplete charge collection. Folkmann et al.[20] have shown that the bremsstrahlung from the "knock on" electrons is most important below 10 keV for a typical case (2 MeV protons on a low Z substrate) rising from 10^{-6} barn/keV at 10 keV to 1 barn/keV at 2 keV. Because the incident particle is so massive, bremsstrahlung from the projectile itslf is small ($\sim 10^{-9}$ barn/keV).   The nuclear microprobe can produce excited states in the nucleus, which decay back to the ground state by emitting gamma rays. These high-energy gamma rays, which are not present in electron-beam-excited samples, can Compton scatter in the detector to produce an additional low-energy background under the characteristic x-ray peak. This is usually not a significant problem unless the sample contains a large mount of an isotope with an extremely high cross section for nuclear reactions such as ^{23}Na.   The final limitation for trace element analysis with a Si(Li) detector is dependent on the quality of the detector itself. At all energies below the full energy peak in a spectrum, there is a relatively uniform back-

ground tail. For a premium quality detctor, the peak to background ratio is usually >1500/1. This can be a problem if there is a very intense high-energy peak in the spectrum, and one is looking for a lower Z contaminant at a level 10^{-3} of the intense line.

Sensitivities for particle induced x-ray emission can often approach 0.1 - 1 ppm for optimal samples. A more reasonable estimate of the routinely available increase in sensitivity relative in electron-beam-excited x-ray spectrometry is probably 2 orders of magnitude. It should be pointed out, however, how complementary x-ray spectrometry is to Rutherford backscattering and nuclear reactions. The x-ray signal can resolve ambiguities in the backscatter spectrum caused by lack of mass resolution for heavier elements. Nuclear reactions can be used for low Z elements where the x-ray spectrometer loses sensitivity because of high backgrounds and absorption in the detector window.

D.   Example (Anodic Oxide on GaAs)

As a simple example of the use of Rutherford backscattering and nuclear reactions to analyze a sample, consider the following case. To develop an MOS technology for III-V compound semiconductors, it is necessary to have a good dielectric on the surface with a low level of surface states. One of the techniques that has been tried involves growing an anodic oxide on the GaAs substrate. A further refinement of the method involves annealing the oxide in various gases such as hydrogen. The problem observed with any processing at elevated temperatures is loss of stociometry at the interface. One of the methods we have tried to avoid high temperature involves laser annealing of the oxide. Anodic oxides on GaAs were irradiated with a pulsed KrF laser ($\tau \approx 70$ ns, $\lambda = 248.4$ nm). At energy fluxes greater than 60 mJ/cm^2, color changes were observed in the oxide indicating a change in the oxide thickness. Total oxygen content in the laser annealed and unannealed portions of the sample were measured with the $^{16}O(d,p_1)^{17}O$ nuclear reaction.

Figure 9 shows a backscattering spectrum obtained with 2 MeV deuterons incident on the GaAs with an anodic oxide. There are several features to be ncted in the backscattered spectrum obtained with an annular surface barrier detector at 175°. There is a broad, thick target yield from the deuterons elastically scattered from the substrate. There is no obvious surface oxygen peak in the deuteron elastic backscattering spectrum. Kinematically this peak should

appear at 1.2 MeV. It is not observed because the cross section for elastic deuteron scattering from oxygen is only 6% of that from Ga or As, and there is a large background of elastic deuterons from deeper layers in the substrate at that energy. There is insufficient energy resolution in the detector to resolve the backscatter from the mass 74 As and mass 69 Ga at the surface. With a high-resolution electrostatic analyzer rather than a simple surface barrier detector, much more detailed analysis of the surface would be possible.[23]

There are four inelastic scattering peaks observed at energies greater than the 2 MeV energy of the incident beam. The peaks at 3.05 and 2.3 MeV are the proton peaks from $^{16}O(d,p_0)^{17}O$ and $^{16}O(d,p_1)^{17}O$ reactions in the surface oxide. The broad peak at 2.9 MeV is from alpha particles from the $^{16}O(d,\alpha)^{14}N$ reaction in the oxide. The peak is broader than the two proton peaks because dE/dx for alpha particles is greater than dE/dx for protons escaping from the oxide. The peak at 3.3 MeV is a proton peak from the $^{12}C(d,p_0)^{13}C$ reaction. The carbon is a contaminant in the anodic oxide growth process. The oxide was grown in a tartaric acid solution. Its presence as a contaminant in the anodic oxide growth process has not been previously reported.

Figure 10 shows the leading edge of the elastic deuteron scattering in more detail and compares the shape to that from native GaAs with no anodic oxide present. The shapes of the spectra are not the same because the density of Ga and As atoms in the oxide is less than pure GaAs. Once the deuterons have penetrated the oxide, the backscattering is the same as from the original GaAs substrate. Notice in the linear plot of the data that a small elastic backscatter peak from the oxygen on the surface is present, but the inelastic proton peaks are a much cleaner analytical signal.

Line scans with the nuclear microprobe across the regions that were laser annealed showed no loss of oxygen relative to the original unannealed oxide. These data in conjunction with optical measurements indicate that the laser annealing process results in a densification of the oxide.

III. PROBE FORMATION

As in all probe-forming systems, Louisville's theorem represents the fundamental limitation for beam current, spot size, angular divergence, and energy spread in the beam of a nuclear microprobe. A typical normalized emittance for

a single-ended Van de Graaff accelerator with duoplasmatron ion source is E_x
$= E_y \sim 1 - 10$ mm mrad MeV$^{1/2}$.   The average current that can safely be accel-
erated down the column of the LASL vertical accelerator i 10 µA. Using these
numbers a d assuming aberration-free optics, it is possible to calculate an
upper iimit on the possible current density in the final probe.

Assume a 1 µm^2 beam of 1 MeV protons from a 10   µA beam of a 1 mm mr MeV$^{1/2}$
accelerator is incident on a specimen with a semidivergence of 50 mr. This
means the beam will be $\sim$ 3 µm diameter at a depth of 20 µm below the surface.
Considering the interaction of the incident beam in the specimen, this is not an
unreasonable upper limit for the divergence of a focused nuclear microprobe.
Then, by Louisville's theorem, the maximum current in the final 1 µm^2 spot is

$$\frac{\left(10^{-3} \text{mm} \times 50 \text{ mr MeV}^{1/2}\right)^2}{\left(1 \text{ mm mr MeV}^{1/2}\right)^2} \times 10 \text{ µA} = 2.5 \text{ nA} \quad . \tag{8}$$

The theoretical upper limit could be a factor of 100 lower depending on the
characteristics of the particular accelerator and ion source. There are two
ways of producing a small diameter beam of particles: collimation and focusing.
Using collimation of a low divergence beam to produce a 3 µm spot would require
a beam divergence of <0.1 mrad if the collimator were 10 mm from the sample.
The resulting beam current for the "typical" accelerator considered above is

$$\frac{\left(10^{-3} \text{ mm} \times 0.1 \text{ mr MeV}^{1/2}\right)^2}{\left(1 \text{ mm mr MeV}^{1/2}\right)^2} \times 10 \text{ µA} = 0.1 \text{ pA} \quad . \tag{9}$$

This beam current is too small to be of use as a nuclear microprobe. However,
at larger spot sizes, the method has been used successfully for spatially
resolved x-ray analysis, and it does have the advantage of overwhelming simplic-
ity. There are several collimated probes in existence today, and they are par-
ticularly useful for analysis of biological specimens in air.[24-28]

To produce a focused nuclear microbeam of <10 µm dimensions requires the
equivalent of one or more lenses to demagnify the beam spot and appropriately
placed collimators to define the object and limit the divergence of the beam.

- 12 -

Since the particles are more massive and of higher energies than electrons in microprobe systems, the problems associated with focusing are somewhat different.

A. Focusing Elements

The general requirements for a final lens of a nuclear microprobe are that the focal length be 10 - 20 cm, the focus should occur at least 5 cm beyond the end of the lens, and the lens should be able to focus particles in the energy range of a few million electron volts per atomic mass unit. Additionally, one would like a lens with low spherical and chromatic aberrations, a large angular acceptance, and simple construction.

There are several possibilities: (1) multiple magnetic quadrupoles, (2) multiple electrostatic quadrupoles, (3) coaxial electrostatic lens, and (4) cylindrically symmetric magnetic lens. Almost all nuclear microprobes in use today use a combination of magnetic quadrupoles for the final lens. The reason for this is that the nonaxially symmetric quadrupole magnetic field is a "strong focusing" field and much more efficient in bending the high-energy heavy ions.

The principal characteristic of a quadrupole lens is that it is converging in one plane and diverging in the orthogonal plane. Therefore, to form a real converging image in both the X and Y planes, one must have at least a doublet lens combination. This is not the appropriate place to discuss quadrupole focusing in detail, but the principal characteristics will be mentioned.[29,30] The doublet is inherently astigmatic; if the two elements are equally excited, the X and Y planes will focus to a line at different distances from the lens. The planes may be made to coincide at a single point by unequal excitation, but then the magnifications in the two planes are different. A symmetric triplet can produce a stigmatic image with a magnification of 1. But in general, a triplet combination of quadrupoles will also be astigmatic. There is a quadruplet arrangement of four equal quadrupoles that can produce a short focus beyond the last lens.[31] This "Russian quad" has been used for several microprobes and is equivalent to a cylindrically symmetric lens.

To obtain a spot size approaching 1 μm with an arrangement of quadrupoles requires very good mechanical and electrical uniformity. Great care must be taken in the design and construction of the quadrupoles. Cooksen et al. have looked at the geometrical, chromatic, and parasitic aberrations of the "Russian

- 13 -

Quad" design.[32] Their quadrupoles have an aperture of 3.84 cm with opposite pole tips uniform to ± 13 μm, and adjacent pole tips uniform to ± 45 μm in a 14.25 mm distance. The four magnets have a common axis to ± 50 μm. The relative rotational alignment was found to be critical, and provision is made to align the quadrupoles to 0.1°.[33] The Heidelberg group took a somewhat different approach with a system with 5 mm aperture, <5 μm tolerances and special treatment of the iron parts of the system to avoid field asymmetries and magnetic stress.[34,35]

The astigmatism usually found with quadrupole lens configurations may appear to be a severe limitation for a nuclear microprobe, but this is not the case. The object focused by the final lens is usually formed by orthogonal pairs of jaws; an asymmetric object can be focused to a symmetric image spot. Also, i · many applications, a symmetric probe spot is not required to obtain useful information. An electrostatic quadrupole triplet of clever design has been used by Augustyniak et al. at Bell Laboratories.[36] The system has a bore diameter of 2 mm and focuses the beam 10 cm beyond the end of the last lens. The design is very compact and has produced a 15 μm spot of 1.5 MeV protons. The authors feel that aberrations caused by imperfections in the ends of the electrodes limit the spot size achievable with this system.

Another kind of electrostatic lens has been used by Krejcik et al. to form a nuclear microprobe.[37,38] The lens is a coaxial doublet that focuses the beam collimated by an annular aperture. The electrostatic field exists between an axial center electrode and outer cylinders. It is possible to focus particles with relatively low voltages. The authors have used the lens to produce a 40 μm spot of 425 keV protons. The lens design is so new that it is not yet known to what extent the spherical aberration of the lens can be minimized. The authors claim that the annular geometry of the entrance aperture "allows much larger beam currents to be focused" in a spot than with a conventional lens. However, a consideration of Louisville's theorem indicates that this is not the case. A conventional lens can image the beam from a high-current density crossover point, while the coaxial electrostatic design images an annular region of large diameter, parallel, low-current density beam.

The LASL nuclear microprobe uses a cylindrically symmetric magnetic lens to focus the beam to its final spot. This type of lens was chosen for its inherent

simplicity and larger angle of acceptance than that possible with a quadrupole multiplet. The conceptual "simplicity" was not purchased without a price; however, the final lens is a superconducting solenoid with a room temperature bore, a considerable complexity.

The magnetic field needed to focus a few million electron volts light ions is considerably higher than for electrons. In general, for magnetic focusing

$$B^2 \sim \frac{ME}{q} \qquad (10)$$

where M is the mass of the particle being focused, E is the energy, and q is the charge.[39]

Comparing the fields required for a 2 MeV proton B_p with a 20 keV electron B_e, we have

$$\frac{B_p(2 \text{ MeV})}{B_e(20 \text{ keV})} = \left(\frac{938 \times 2}{0.512 \times 0.02} \right)^{1/2} = 428 \quad . \qquad (11)$$

Simple scaling up of the lens for an electron microprobe will not work because even special iron saturates at 2.5T, and conventional magnetic lenses without iron cannot be made with current densities of 10^4 A/cm^2 without overheating.

A flat pancake superconducting solenoid was fabricated in a cryostat with a horizontal room temperature bore for use as the final lens. The principal characteristics of the magnet are listed in Table II.

The field of the superconducting solenoid is reasonably close to the Glaser model of a symmetric lens,

$$B(Z) = \frac{B_0}{1 + \left(\frac{z}{a} \right)^2} \quad , \qquad (12)$$

where B_0 is the field at the center of the lens, and a is the distance between the center and the points where the axial field equals $B_0/2$. Figure 11 compares the superconducting solenoid with a Glaser field where a = 6.5 cm.

The Glaser field has the property that its aberrrations can be solved analyt-ically.[40] The calculated spherical and chromatic aberrations for the equiva-lent Glaser field are C_S = 14 cm and C_C = 9.3 cm.

B.   Beam Line Optics

Since the typical normalized emittance of a Van de Graaff accelerator is 1 - 10 mm mr $MeV^{1/2}$ and the maximum divergence acceptable in a focused spot is < 50 mr, one must somehow limit the emittance of the machine to produce a 1 μm focused spot on target. The choice of collimator placement and type put dif-ferent constraints on the beam line. Several different combinations of colli-mators and focusing elements have been tried.[32-36,41-42]   The LASL microprobe uses the superconducting solenoid to demagnify by 10 the object formed by crossed pairs of temperature controlled microjaws.

Figure 12 shows a schematic diagram of the LASL microprobe beam line with an optical analog. The components shown in the optical analog are common to most nuclear microprobes. The Van de Graaff accelerator may be viewed simply as a source of variable energy particles. The LASL accelerator has a R = 2 m radius 90° bending magnet to momentum analyze the beam. The variable entrance and exit slits for the 90^6 magnet are symmetrically located at the 2R posi-tion. The magnet is double focusing at this position. The object and image slit widths for the bending magnet determine the energy resolution of the beam, and the beam current on the image slits provides the feedback signal to regulate the terminal voltage of the accelerator. The quadrupole triplet Q_{123} is an emittance matching element to change the divergence of the beam to match the acceptance of the final lens. Crossed pairs of microslits are located at the focus of the triplet. They define the object that is demagnified by the final lens. For the LASL microprobe, this is the final emittance limiting aperture. A set of divergence limiting slits is located in front of the final lens.

The quality of the final image spot is determined not only by the chromatic and spherical aberrations of the final lens, but also by the relative amount of slit scattering that occurs at the object slits and the vacuum between the ob-ject slits and the specimen. Nobiling et al. have made an excellent study of slit scattering and the effects of residual gas scattering on the quality of collimated beams of nuclear particles.[43] Figure 13 points out the nature of the problem and the solution proposed by the Heidelberg group. The focused beam

will have a diffuse halo around it limiting the peak-to-background ratio of the spot. The halo is due to particles that have tranversed the transparency zone of the slit edge or scattered from residual gas atoms between the object slits and the target. The Heidelberg design requires the incident beam to undergo a double scattering event to be misfocused by the final lens. The transparency zone is reduced by making the edge at a shallow angle with minimum surface roughness.

The LASL microprobe uses jaws of gold-plated copper that have been machined with a single-crystal diamond tool bit. Examination of the edge with an SEM indicates an edge roughness of less than 0.1 µm. The total opening of the microslits is controlled by varying the temperature of copper cold fingers mounted in a temperature-controlled six-way cross.

Figure 14 is a schematic of the system. The absolute opening can be controlled from 0 - 120 µm ± 0.4 µm independently in the X and Y directions. We have not had sufficient experience to determine whether radiation damage to the microjaws will be a major problem. It may be necessary to switch to a less delicate jaw design similar to that used by Cooksen et al. at Harwell.[32]

The vacuum system of the LASL microprobe is separated from the accelerator vacuum by dual differential pumping ports located between the quadrupole triplet and the object slits. The beam line before the triplet is turbomolecular pumped and typically operates at 2×10^{-6} torr. The beam line after the differential pumping ports is all metal sealed, bakeable to 250°C, and ion pumped. Normal operating pressure in the beam line and scattering chamber is 7×10^{-9} torr.

Mechanical stability is very important in the performance of a nuclear microprobe, since any motion of the object slits relative to the final lens and target results in motion of the spot on the target. To first order, the motion is reduced by the magnification factor; but the constraint is tight considering the large distance between the object and the image and the high mechanical vibration environment typical of a nuclear physics laboratory. The LASL microprobe has the object slits, final lens, and scattering chamber mounted on a single re-enforced concrete block, 2 m x 1.2 m x 0.8 m, isolated from the floor.

The electrical stability of the beam line components can also be a limiting factor in microprobe performance. The power supplies for steerers and quadrupoles are not usually high-stability, low-ripple supplies similar to those

used in a SEM or electron microprobe. Legge et al. have modified current supplies with 1000 ppm stability and 100 ppm ripple to have 5 ppm stability and 10 ppm ripple for use on the Melbourne proton microprobe.[41] The LASL microprobe uses a power supply with 0.01% stability and ripple for the superconducting solenoid. However, to align the beam, there are three sets of magnetic steerers located at the exit slits of the 90° magnet, immediately before the quadrupole triplet, and just after the microjaws defining the object for the solenoid. These steerer power supplies and the supplies for the triplet do not have the required current stability for 1 μm position resolution. This is the main limitation for the LASL probe now, and this part of the system is being redesigned and upgraded.

The nuclear microprobes in existence today are single beam lines at Van de Grauff accelerator laboratories. As such they usually represent compromises that are far from optimal for microprobe work. For example, the LASL microprobe has a serious problem with matching the divergence of the beam to the acceptance of the 90° bending magnet. There is insufficient space between the exit of the machine and the object slits of the magnet to put an emittance matching element such as a quadrupole doublet. One must therefore run with ~ 20% of the accelerated beam out of the 90° magnet for adequate energy resolution in the beam. This particular compromise may be unique to the LASL probe but is probably not untypical of the compromises being made with the other microprobes. This should be kept in mind when comparing the systems in existence today.

Table III shows the main parameters defining several of the microprobes around the world. The phase space may be considered a figure of merit for the various systems as pointed out by Cooksen from work of Heck.[32,44] The distance labeled drift space refers to the distance between the object slits and the center of the lens. The maximum acceptance is the size needed to produce a 3 μm diameter spot. The specifications listed under comments are the minimum size spot and maximum current density reported.

The relatively large phase space acceptance for the LASL microprobe is due to the large angular acceptance of the lens compared to quadrupole systems. A quadrupole focuses in one plane and defocuses in the orthogonal plane; the angular acceptance must be restricted to prevent the beam hitting the magnet pole pieces. Some high-precision quadrupoles in use for microprobes have been

- 18 -

made with relatively narrow apertures. The LASL solenoid has a room temperature
bore of 19 mm and a free bore of 14 mm inside the vacuum system. A solenoidal
field is always a converging field.

Figure 15 shows the intensity of backscattered deuterons om a thin gold
evaporation, 80 nm, on a silicon substrate. The scan across tne edge of the
evaporation indicates a spot size of 5.2 μm FWHM. This was obtained by assuming
a gaussian intensity distribution for the spot and a step function for the gold
thickness. The object slits were set at ±20 μm in the X and Y directions. The
beam accelerated down the column of the machine was 3 μA of 2 MeV negative
deuterons. The object and image slits were set for $\Delta E/E = 4 \times 10^{-4}$. The beam
current at the image of the bending magnet was 170 nA, which was incident on the
microjaws. The beam current on target was 4 nA. The beam divergence into the
solenoid was ±2 mrad in the X and Y directions. Considering the large-phase

acceptance of the system, one may ask why the current density of
190 pA/μm^2 is so low. The answer lies in the 'act that only 3 μA was accel-
erated in the machine, and 94% of that beam was lost in the energy analysis part
of the system before it got to the microprobe. The inherent optical mismatch
between the exit of the machine and the entrance to bending magnet is the prob-
lem.

The ±20 μm object slits should have produced a 4.1 μm image spot. The
larger 5.2 μm spot may be due to chromatic and spherical lens aberrations, but
I don't think so because the spot size did not vary as expected when changing
the angular acceptance of the system. The measurement of chromatic and spheri-
cal aberration coefficients will be attempted after upgrading the beam line
power supplies.

C.   Data Acquisition

The method of moving the beam relative to the sample varies with the par-
ticular microprobe and is closely related to the data-acquisition system. There
are two basic approaches: 1) postdeflection of the beam after focusing and 2)
moving the specimen relative to the beam. Since the resolution of nuclear mic-
roprobes (1 - 10 μm) is relatively poor compared to a SEM, and the data-
acquisition time per pixel is longer, mechanical scanning of the specimen
relative to the beam doesn't represent as serious a drawback as it may at first
appear. Coming from a nuclear physics background rather than a microscopy back-

ground, the data acquisition is usually a variation of standard nuclear physics techniques rather than a variation of microscopy technique.

Perhaps the simplest data acquisition consists of recording a single signal by synchronously scanning the beam and a CRT and using a camera to record the position of events of interest. The method is familiar to SEM users and produces elemental maps similar to those from a SFM x-ray spectrometer combination. There is, however, a problem associated with the inherent instability of nuclear microprobe beam currents. One would like to cor.ider the Van de Graaff accelerator a simple source of high-energy ions cf constant energy and intensity; this is ot the case. In contrast to an electron beam instrument, long-term current : ability of 0.1% is not usually possible. The charging system, fast regulation, slow regulation, and complex ion source all contribute to beam current instability. Ten per cent stability for one-half hour would be good; stability is commonly much worse. Any system using externally generated X and Y sweeps to move the beam requires repeated scanning of the area to average over the fluctuating beam current for quantitative results. The alternative way of getting quantitative results is to count for a preset integrated charge at a pixel point before moving to the next position on the specimen.

At its most general, the data consist of a number of events, where an event is characterized by a multidimensional number. For example, suppose a proton is backscattered from a specimen. The event would consist of three or more numbers: X position, Y position, energy of the proton, and perhaps additional numbers required to identify the detected particle as a proton. One method of data acquisition is multiparameter event storage in which the multidimensional number associated with each event is stored in the memory of a computer or written to a mass storage unit such as a disk or magnetic tape. After the data are acquired, the memory or mass storage unit can be scanned by the computer with various cuts on the data, that is, requiring the events to satisfy certain constraints. In this way, two-dimensional elemental maps, line scans, position averaging, and background subtractions can be performed with the computer after the data have been obtained. Legge and Hammond discuss this method used with their microprobe.[45]

One of the problems associated with complete event storage is that the computer itself can limit data retrieval rates. The computers used at most nuclear

physics laboratories are limited to incoming data rates of ~100 K counts/s for singles data. Multiparameter event storage rates are significantly less than this, particularly if the mass storage medium is magnetic tape. The other problem is the huge amount of data that must be stored for relatively little information. For example, if a three word event (X, Y, E) is stored for a 128 x 128 area scan on a 2.5×10^6 word disk, only about 50 events per pixel point can be stored on the disk. The problem is the redundancy associated with storage of the position information.

The LASL microprobe uses the computer-based data-acquisition system shown in Fig. 16. The specimen is moved relative to the beam by computer-controlled piezoelectric drivers (Burliegh Inchworms). The specimen can be positioned in two directions over a 2 cm x 2 cm area to the nearest 2 μm ± 0.5 μm. The maximum speed is ~250 μm/s. All data input and output are handled by the CAMAC interface for the Mod Comp computer.

Data acquisition is based on the concept of complete storage of spectral information at each pixel without event storage. Quantitative results are obtained by counting for a preset integrated charge at each pixel. A complete spectrum from the x-ray spectrometer and the backscatter detector is recorded on magnetic tape at the end of each pixel point. During actual data acquisition, the computer is used as multiple multichannel analyzers. The user can define up to 72 gates or energy windows on his two incoming spectra, and the resulting integrated counts per pixel can be stored in memory locations corresponding to the position. One can make 72 simultaneous line scans in the memory of the computer, which are recorded on magnetic tape at the end of each line. The line scans are cuts on the multiparameter data that in many cases are adequate for solving a problem. However if the gates were set incorrectly, a line scan in a different direction is required, or spectral averaging over a defined area is required; the magnetic tape can be sorted with new cuts since complete event recovery, except for time sequence, is possible. The computer-based data acquisition has great flexibility and can be modified to suit the particular problem. One is limited only by one's imagination and stamina as a programmer.

D.   Applications

The nuclear microprobe has mainly been applied to two types of problems: light element detection in metallurgical specimens using nuclear reactions and

PIXE analysis of biological, metallurgical, and geological samples. RBS analysis with a microprobe has been limited to a few cases of problems with semiconductors and electrical components,[46,47] but this use is expected to increase in the future.

The group at Harwell has been most active in the use of the nuclear microprobe for light element depth profiting in metallurgical samples. One technique that they have found very useful involves beveling the surface at an angle so that a linear scan across the bevel corresponds to a changing depth scale. Cooksen's review paper has a table that lists microbeam analyses carried out with a nuclear microprobe using reactions.[32] The breadth of problems covered m   nsed by the following partial list: hydrogen in metals, deuterium in F.   lows, LiOH corrosion in steel, Be diffusion in copper, boron in metals, ^{12}C in metals, nitrided metals, metal oxides, ceramic nuclear fuel oxides, and corrosion layers.[48-53]

Since the cross section for x-ray production is so high, the applications of PIXE with a microprobe are easier to achieve. The review articles discuss the PIXE technique in detail, and no attempt at a comprehensive review will be made. Biological applications range from studies of human hair, to rat kidney, to pollen tubes.[54-56,35,26,24] The problems, as might be expected from electron-microprobe experience, are primarily associated with specimen preparation. Since the advantage of PIXE is its greater sensitivity, the problems of specimen preparation will be more difficult. Contamination and elemental migration during preparation and analysis must be carefully monitored. Many biological analyses have been carried out in air with collimated beams where the problems of specimen heating and handling are easier to manage.

Geological applications of PIXE with a microprobe are demonstrated by studies of trace elements in mineral grains of lunar basalt.[57,35] The work is a good example of the advantage of PIXE relative to electron-beam-excited studies of the same samples. The proton microprobe was able to identify quantitatively trace elements that could not be detected at all with the electron microprobe.

Some of the most exciting and useful developments will come from combined uses of PIXE and RBS or nuclear reactions with a microprobe. Harwell has done extensive work with metallurgical specimens comparing elements such as Ti, Cr,

Ni, Fe, etc., detected with x rays and light elements such as C, O, N, etc., detected with nuclear reactions.[58,32] The x-ray spectrometer is an excellent adjunct to RBS and can be used to untangle ambiguities in the backscattering spectrum. The work of Bell Laboratories with GaAs is an interesting example.[59]

IV. CONCLUSIONS

The nuclear microprobe is slowly maturing in the nuclear physics laboratories of several Van de Graaff accelerators. There has been no strong commercial development by a single company to provide a complete system. Considering the cost of the accelerator itself, such commercial development may never come. However, there are now enough nuclear probes in existence to make them a useful, available tool to be considered by the investigator interested in problems of the near surface region of materials. The RBS and nuclear reactions offer nondestructive analytic signals that are uniquely suited to many problems. The quantitative and relatively unambiguous interpretation of the data makes them useful for checking other surface analytical techniques that depend on the destruction of the sample for depth analysis. The 2 orders of magnitude increased sensitivity of PIXE relative to the electron microprobe should find an interested and waiting group of investigators.

The future development of nuclear microprobes will probably follow the development of electron beam instruments, but more slowly because of a lack of competitive commercialization. For the convenience of the user, secondary electron imaging will be a significant advance. Younger and Couksen have a secondary electron detector on their probe, and it greatly simplifies specimen positioning and focusing.[60] There may be some interest in using different analytical signals with a nuclear microprobe, but for the immediate future, I see an increased use of PIXE with nuclear reactions and RBS. The final development will be in the area of improved ion optical performance. Spatial resolution of $< 1\,\mu m$ is almost here with single-stage defocusing. The addition of another lens and complete optimization of the accelerator and beam line will probably be required for resolution significantly better than $1\,\mu m$. The second lens, however, may not be analogous to that of electron probes, but rather a multiplet or higher order n-pole combination to reduce spherical and chromatic aberrations in a subsequent round lens.

- 23 -

The unique features of a nuclear microprobe should be kept in mind when considering whether or not it is suitable for a particular problem. The results are quantitative without reference to standards of similar composition. This applies to both the elements present and the depth distribution of those elements. The sample does not have to be ion milled or etched away; you may not have 0.1 monolayer sensitivity, but you don't have the uncertainties of unknown beam specimen interactions also. The light element and isotope sensitivity obtained with nuclear reactions is unequaled particularly the possibilities for hydrogen depth profiting.[61,62] The 1 ppm sensitivity of PIXE analysis requires a greater degree of care in specimen preparation and handling than 1000 ppm sensitivity of electron microprobes. Questions of specimen heating and damage will ultimately determine how useful the increased sensitivity will be for microanalysis. Since a Van de Graaff accelerator and microprobe beam line is inherently more complex than an electron microscope, the use of a nuclear microprobe will probably always be restricted to those problems for which it offers unique capability. There is little possibility of nuclear microprobes becoming as ubiquitous as SEM's.

ACKNOWLEDGMENTS

TABLE 1
SELECTED NUCLEAR REACTIONS FOR LIGHT ELEMENT ANALYSIS

Target	Reaction	Q Value (MeV)	Cross Section (mb/sr)	Incident Energy (MeV)
^2H	$^2H(d,p)^3H$	4.03	5.2	1.0
^7Li	$^7Li(p,\alpha)^4He$	17.35	1.5	1.5
^9Be	$^9Be(d,\alpha)^7Li$	7.15	1	1.6
^{11}B	$^{11}B(p,\alpha_1)^8Be$	5.65	90	0.65
^{12}C	$^{12}C(d,p)^{13}C$	2.72	35	1.2
^{14}N	$^{14}N(d,\alpha_1)^{12}C$	9.15	1.3	1.2
^{16}O	$^{16}O(d,p_0)^{17}O$	1.92	0.7	0.9
^{16}O	$^{16}O(d,p_1)^{17}O$	1.05	4.5	0.9
^{18}O	$^{18}O(p,\alpha)^{15}N$	3.98	15	0.7
^{19}F	$^{19}F(p,\alpha)^{16}O$	8.11	0.5	1.3
^{23}Na	$^{23}Na(p,\alpha)^{20}Ne$	2.38	4	0.6

For purposes of materials analysis, the spectroscopy of the light nuclei is sufficiently well known to make the data analysis tractable.

TABLE 2

CHARACTERISTICS OF LASL SUPERCONDUCTING SOLENOID FINAL LENS

Type   :   Multifilament NbTi

                     NbTi:Cu = 1:1.3

                     Epoxy potted

Dimensions   :   5-cm bore length

                     Three-stage winding

$r_1 = 2.5$ cm

$J_{max} = 1.01 \times 10^4$ A/cm^2

$r_2 = 5.75$ cm

$J_{max} = 1.43 \times 10^4$ A/cm^2

$r_3 = 9.65$ cm

$J_{max} = 2.46 \times 10^4$ A/cm^2

$r_4 = 15.8$ cm

Maximum current   :   69.56 A

Maximum field on axis: 80 kG

l. He consumption :   1.5 ℓ/h at maximum field

Inductance   :   45.2 Henries

Charge rate   :   3 kG/min

Manufacturer   :   Intermagnetics General

TABLE 3

COMPARISON OF NUCLEAR MICROPROBES

System	Magnification		Max Acceptance				Phase Space	Drift Space	Comments
	M_x	M_y	X	Y	$\Delta\theta_x$	$\Delta\theta_y$	$m^2 mrad^2$	m	
			$\pm$ µm		$\pm$ mrad				
Harwell "Russian Quad"	0.18	0.18	8.5	8.5	0.62	0.4	18	3.9	First focused probe
Heidelberg Doublet	0.21	0.038	7	40	0.7	0.39	76	1.9	1.5 µm, 30 pA/µm^2
Karlsruhe Doublet	0.43	0.034	3.5	44	1.17	0.47	83	2.7	2.5 µm, 60 pA/µm^2
Harwell Triplet	0.114	0.053	13.2	28.4	0.26	0.64	52	3.9	2 x 3 µm^2, 150 pA/µm^2
LASL Solenoid	0.1	0.1	15	15	2	2	900	1.1	5.2 µm, 190 pA/µm^2

REFERENCES

1. J. Mayer, A. Turos, "Comparison of Surface Layer Analysis Techniques," Thin Solid Films, 19, 1973, 1-10.

2. W. K. Chu, "Material Analysis by Nuclear Backscattering," Chapter 2, new Uses of Ion Accelerators, ed. J. F. Ziegler, Plenum, New York USA, 1975.

3. W. K. Chu, M. Nicolet, J. Mayer, Backscattering Spectrometry, Academic Press, New York, USA, 1977.

4. L. C. Northcliffe, R. F. Schilling, "Nuclear Data Tables, A7, 1970, 233.

5. H. H. Anderson, J. F. Ziegler, Hydrogen Stopping Powers and Ranges in all Elements, Pergamon, New York, USA, 1977.

6. J. F. Ziegler, Helium Stopping Power and Ranges in all Elemental Matters, Pergamon, New York, USA, 1977.

7. P. W. Keaton, P. S. Peercy, B. L. Doyle, C. J. Maggiore, "A New Technique for Backscattering Analysis," Proceedings IV Int. Conf. on Ion Beam Analysis, NIM, 1980.

8. U. Fano, Annual Rev. Nucl. Science, 131, 1963, 1.

9. W. H. Bragg, R. Kleeman, Phil. Mag., 10, 1905, 318.

10. J. S. Y. Feing, W. K. Chu, M. A. Nicolet, "Bragg's Rule Study in Binary Metal Allows and Metal Oxides for MeV ^{4}He Ions," Thin Solid Films, 19, 1973, 227-238.

11. Rutherford, Phil. Mag., 21, 1911, 669.

12. J. W. Mayer, E. Rimini, Ion Beam Handbook for Material Analysis, Academic Press, N.Y., USA, 1977, Chapters 2, 4, 5.

13. O. Meyer, G. Linker, F. Kappeler, Ion Beam Surface Layer Analysis, Plenum Press, New York, USA, 1976.

14. E. L. Wolicki, "Material Analysis by Means of Nuclear Reactors," Chap. 3 of New Uses of Ion Accelerators, Ed. J. F. Ziegler, Plemun, New York, USA, 1975, 159-228.

15. G. Ansel, J. Nadai, E. D'Artemare, D. David, E. Girard, J. Moulin, "Microanalysis by the Direct Observation of Nuclear Reactions Using a 2 MeV Van de Graaff," NIM, 92, 1971, 481.

16. J. A. Moore, I. V. Mitchell, M. J. Hollis, J. A. Davies, L. M. Howe, "Detection of Low Mass Impurities in Thin Films using MeV Heavy Ion Elastic Scattering and Coincidence Detection Techniques," J. Appl. Phys., 46, 1975, 52.

17. C. M. Leaderer, V. S. Skipley, eds., <u>Table of Isotopes</u>, Wiley, New York, USA, 1976, 23.

18. T. A. Cahill, "Ion Excited X-ray Analysis of Environmental Samples," Chap. 1., <u>New Uses of Ion Accelerators</u>, Ed. J. Ziegler, Plenum, New York, 1975.

19. S. A. E. Johansson, T. B. Johansson, "Analytical Applications of Particle Induced X-ray Emmission," NIM, <u>137</u>, 1976, 473-516.

20. F. Folkman, C. Gaarde, T. Huus, K. Kemp, "Proton Induced X-ray Emission as a Tool for Trace Element Analysis," NIM, <u>116</u>, 1974, 487-499.

21. F. Folkman, "Analytical Use of Ion Induced X-rays," J. Phys., <u>E8</u>, 1975, 429-444.

22. F. S. Goulding, J. M. Jaklevic, "XRF Analysis--Some Sensitivity Comparisons between Charged Particle and Photon Excitation," NIM, <u>142</u>, 1977, 323-332.

23. M. Hage-Ali, P. Siffert, "Compound Semiconductors Surface Characterization by High Resolution Rutherford Backscattering," NIM, <u>166</u>, 1979, 411-418.

24. R. E. Shroy, H. Kraner, K. Jones, "Proton Microprobe with Windowless Exit Port," NIM, <u>157</u>, 1978, 163-168.

25. P. Horowitz, L. Grodzins, "Scanning Proton Induced X-ray Microspectrometer in an Atmospheric Environment," Science, <u>189</u>, 1975, 795.

26. P. Horowitz, M. Aronson, L. Grodzins, W. Ladd, J. Ryan, G. Merrian, C. Lechene, "Elemental Analysis of Biological Specimens in Air with a Proton Microprobe," Science, <u>194</u>, 1976, 1162.

27. L. Grodzins, P. Horowitz, J. Ryan, <u>Proc. Conf. Sci. and Industrial App. of Small Acc.</u>, ed. J. Duggan, I. Morgan, IEEE, New York, 1976, 75.

28. G. V. Gentry, T. A. Cahill, H. Fletcher, H. Kaufman, L. Medskev, J. Nelson, R. Flocchini, "Evidence for Primordial Superheavy Elements," PRL, <u>37</u>, 1976, 11-15.

29. P. W. Hawkes, Quadrupoles in Electron Lens Design, Academic Press, New York, USA, 1970, Chap. 4, 5.

30. E. Regenstreif, "Focusing with Quadrupoles, Doublets, and Triplets," Chap. 2.4, ed. A. Septer, <u>Focusing of Charged Particles</u>, Academic Press, New York, USA, 1967: P. W. Hawkes, "Lens Aberrations," Chap. 2.5.

31. A. Dymnikov, T. Fishkova, S. Yavor, "Effect of Geometrical Parameters on Optical Characteristics of a System of Four Quadrupole Lenses Similar to an Axisymmetric Lens, Soviet Phy-Tech Phy., <u>10</u>, 1965, 340.

32. J. A. Cooksen, "The Production and Use of a Nuclear Microprobe of Ions at MeV Energies," NIM, <u>165</u>, 1979, 477-508.   (There is a misprint in this paper, a 400 mesh grid rather than 200 mesh grid was used for spatial calibration. The spot sizes listed are correct.)

33. J. Cooksen, F. Pilling, "A 3 MeV Proton Beam of Less Than Four Microns

Diameter," AERE R 6300, 1970.

34. F. Bosch, A. El Goresy, B. Martin, B. Povh, R. Nobiling, D. Schwalm, K. Traxel, "The Heidelberg Proton Microprobe," NIM, 149, 1978, 665-668.

35. F. Bosch, A. El Goresy, W. Herth, B. Martin, R. Nobiling, B. Povh, H. D. Reiss, K. Traxel, "The Heidelberg Proton Microprobe," Nucl. Sci. App., 1, 1980, 1.

36. W. M. Augustyniak, D. Betteridge, W. L. Brown, "A Miniature Electrostatic Lens for Forming MeV Millbeams," NIM, 149, 1978, 669-673

37. P. Krejcik, R. L. Dalglish, J. C. Kelley, "An Electrostatic Coaxial Probe Forming Lens Suitable for High-Energy Ion Beams," J. Phys. D: Appl. Phys., 12, 1979, 161-167.

38. P. Krejcik, J. C. Kelly, "A New Electrostatic Ion Microprobe System," NIM, Proc. 4th Int. Conf. on Ion Beam Anal., Aarhus, 1979.

39. P. Grivet, Electron Optics, 2nd Ed., Pergamon Press, Oxford, England, 1972, Chap. 7, 9, 10.

40. A. B. El Kareh, J. C. J. El-Kareh, Electron Beams, Lenses, and Optics, Academic Press, New York, USA, 1970, Chap. 7, 10, 14.

41. G. J. F. Legge, C. D. McKenzie, A. P. Mazzolini, "The Melbourne Proton Microprobe," J. of Micros., 117, Pt. 2, 1979, 185-200.

42. D. Heck "Kernforschungszentrum Karlsruhe KFK Report 2379," 1976, 108.

43. R. Nobiling, Y. Cwelekoglu, B. Povh, D. Schwalm, K. Traxel, "Collimation of Ion Beams to Micrometer Dimensions, NIM, 13C, 1975, 325-334.

44. D. Heck, "Kernforschungszentrum Karlsruhe Report KFK 2380," 1978, 115.

45. G. J. F. Legge, I. Hammond, "Total Quantitative Recording of Elemental Maps and Spectra with a Scanning Microprobe," J. Micros., 117, Pt. 2, 1979, 201-210.

46. K. Schmid, H. Miller, H. Ryssel, I. Ruge," Investigation of Lateral Damage Effects of Ion Implanted Layers by Backscattering Techniques," Thin Solid Films, 19, 1973, 313-318.

47. P. Bayerl, P. Eichinger, "A Shutter Controlled Microbeam Combined with Scanning System for Two Dimensional Backscattering Images," NIM, 149, 1978, 663-664.

48. J. Cooksen F. Pilling, "The Use o Focused Ion Beams for Analysis Thin Solid Films, 19, 1973, 381-385.

49. J. McMillan, P. Hirst, P. Pummery, J. Huddleston, T. Pierce, "Recent Developments in Nuclear Microprobe Analysis, Particularly the Determination of Beryllium Distributions in Metals," NIM, 149, 1978, 83-91.

50. J. A. Cooksen, J. W. McMillan, T. B. Pierce, "The Nuclear Microprobe as an

Analytical Tool," J. of Radioanalytical Chemistry, <u>48</u>, 1979, 337-357.

51. J. F. Singleton, N. Hartley, J. Radioanal. Chem., <u>48</u>, 1979, 317.

52. T. B. Pierce, J. W. McMillan, P. F. Peck, and I. G,. Jones, NIM, <u>118</u>, 1974, 115.

53. C. Olivier, J. W. McMillan, and T. B. Pierce, NIM <u>124</u>, 1975, 289.

54. C. A. Cookson, and F. D. Pilling, Phys. Med. Biol. <u>20</u>, 1975, 1015.

55. G. J. F. Legge, Proc. Second Aust. Conf. on Nucl. Tech. of Anal., 1978, 18.

56. A. P. J. Mazzolini and G. J. F. Legge, Proc. Second Aust. Conf. on Nucl. Tech. of Anal., Lucas Heights, 1978, 28.

57. F. Bosch, A. El Goresy, B. Martin, B. Povh, R. Nobiling, D. Schwalm, K. Traxel, "The Proton Microprobe: A Powerful Tool for Nondestructive Trace Element Analysis," Science, <u>199</u>, 1978, 765-768.

58. T. B. Pierce and J. Huddleston, NIN <u>144</u>, 1977, 231.

59. R. L. Kauffman, L. Feldman, J. M. Poate, R. P. Change, "Analysis of Plasma-grown GaAs Oxide Films," APL, <u>30</u>, 1977, 319-321.

60. P. Younger, J. Cooksen, "A Secondary Electron Imaging System for a Nuclear Microprobe," NIM, <u>158</u>, 1979, 193-198.

61. E. Ligeon and A. Guivarc'h "Radiation Effects," <u>22</u>, 1974, 101.

62. J. Ziegler et al., NMI <u>149</u>, 1978, 9.

63. G. Bonani, M. Suter, H. Jung, Ch. Stoller, W. Wolfi, "A Digitally Controlled Scanning Microprobe for Protons and Heavy Ions," NIM, <u>157</u>, 1978, 55-63.

FIGURE CAPTIONS

Fig. 1. Possible results of the interaction of a few MeV light ions with a
         specimen.

Fig. 2. Geometry for a Rutherford backscattering experiment. The incident
         particle M_1 is elastically backscattered from the nucleus M_2
         located a distance t below the front surface.

Fig. 3. Generalized geometry for backscattering from a high-Z film on a low-Z
         substrate and the observed energy spectrum of backscattered particles.

Fig. 4. Stopping power of ^{4}He particles in gold.

Fig. 5. Effective scattering cross section in counts A for 1 MeV ^{4}He
         particles from target nuclei at a back angle of 160°. A = Q$\sigma\Omega$Nt where
         Q = 6.25 x 10^{12} (1   μC of ^{4}He ions), Ω = 10^{-3} str, and
         Nt = 10^{16} target atoms/cm^2.

Fig. 6. Kinematic factor K = E'/E for elastic scattering of ^{4}He at a back
         angle of 160°.

Fig. 7.   Schematic representation of the $^{16}O(d,p)^{17}O$ reaction.   If the ^{17}O
nucleus is left in the ground state, the Q value of the reaction of
1.92 MeV.   If the ^{17}O nucleus is left in the first excited state, the
Q value is 1.05 MeV.   The nucleus then decays to the ground state by
emitting an γ ray.

Fig. 8.   Cross section vs incident energy for a typical nuclear reaction in a
low-Z nucleus.   The resonance behavior complicates the depth
distribution information from thick targets.

Fig. 9.   Backscattering spectrum of 2 MeV deuterons on GaAs with an anodic
oxide.   No particle discrimination was used to separate the proton and
alpha particle reaction products from the elastically scattered
deuterons.

Fig. 10.   Comparison of 2 MeV deuteron backscattering spectra from GaAs with and
without an anodic oxide on its surface.

Fig. 11.   Comparison of the LASL superconducting solenoid with a Glaser field.

Fig. 12.   Schematic diagram of the LASL nuclear microprobe beam line.

Fig. 13. Slit scattering and its minimization by careful slit design.

Fig. 14. Temperature controlled microslits. Two thermistors measure the temperature of the copper heat sinks. A variable set point circuit controls the temperature by varying the flow of cooling water to the copper rods.

Fig. 15. Backscattered deuteron intensity from a gold film on a silicon substrate.

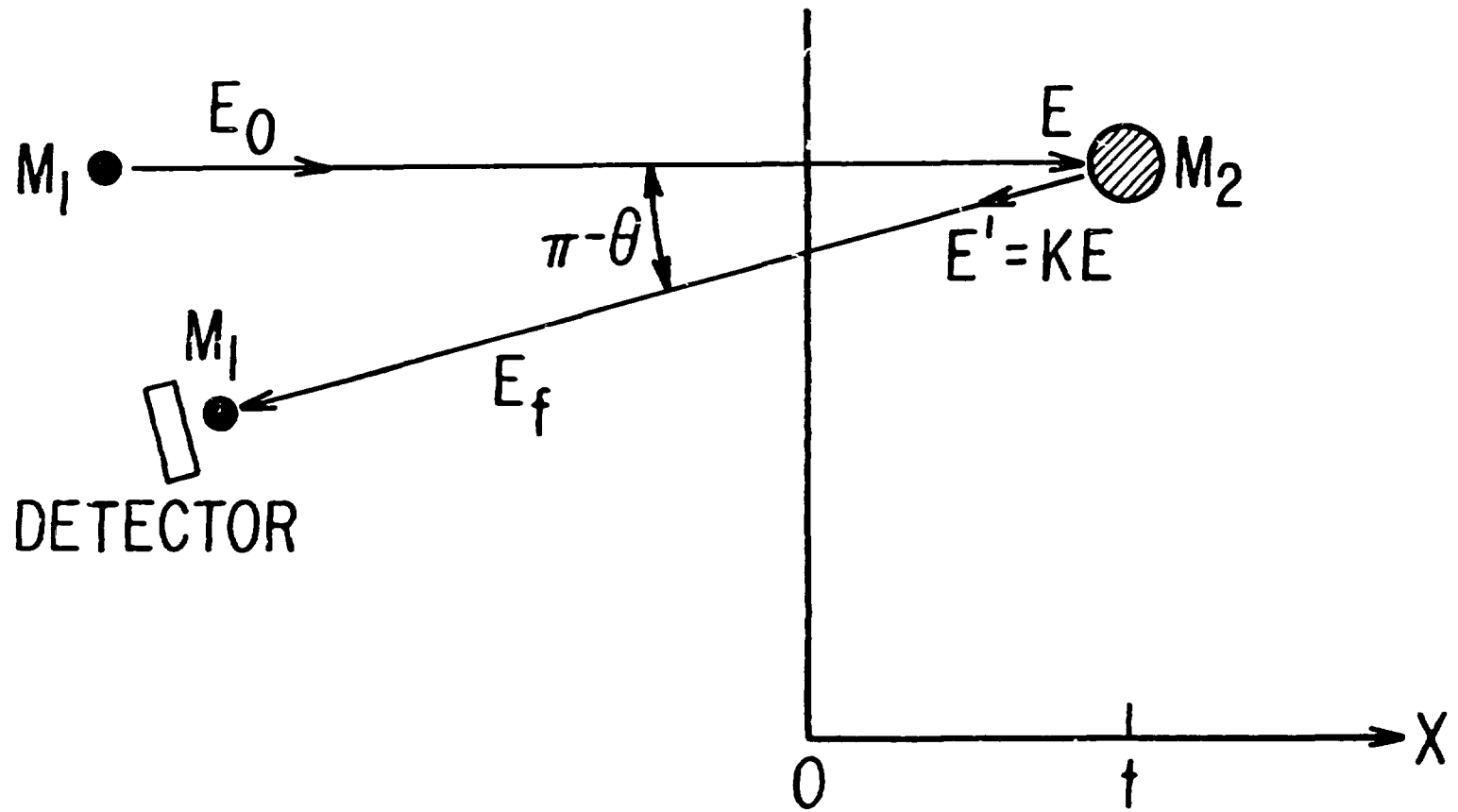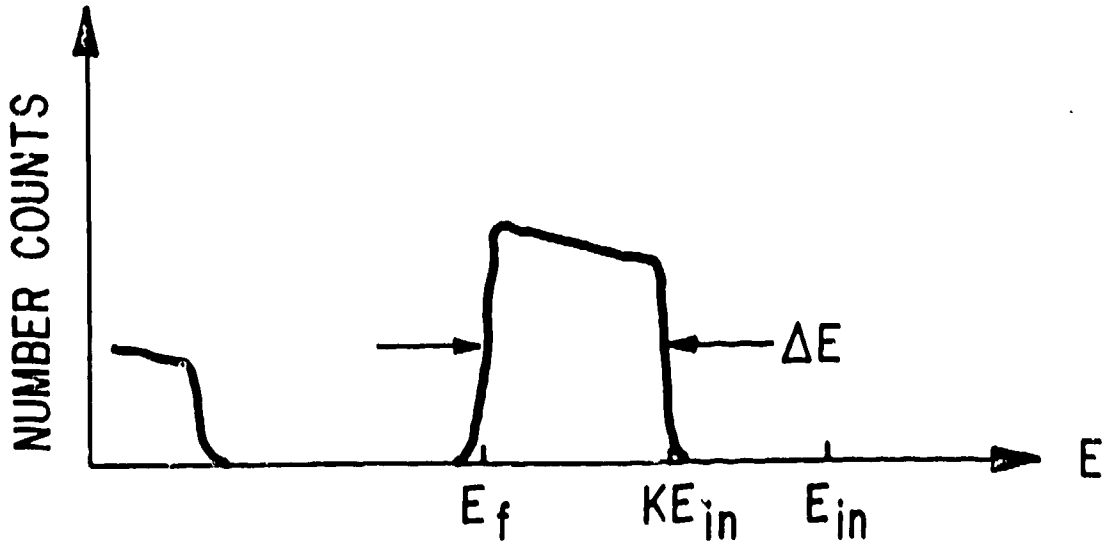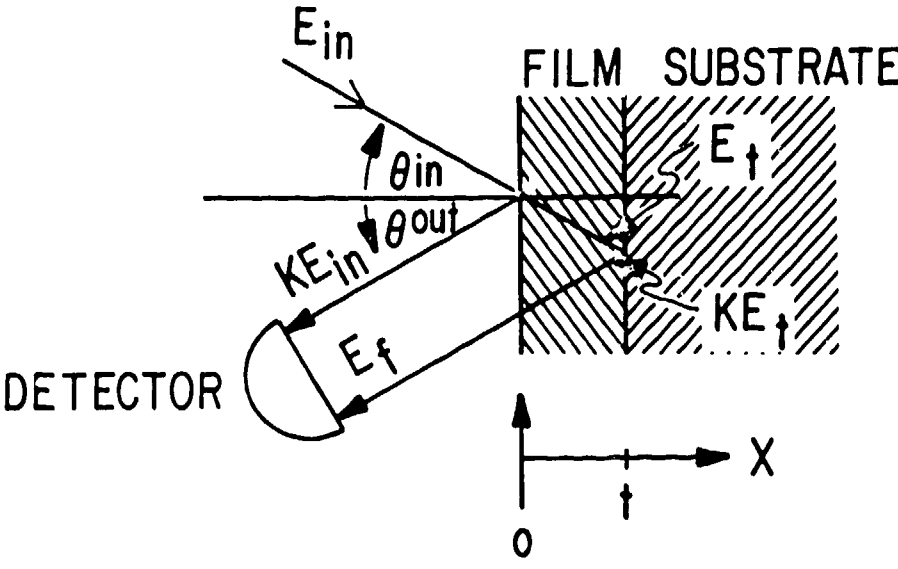Fig. 16. Computer-based raster generation and data acquisition for the LASL microprobe.

SECONDARY ELECTRONS

OPTICAL PHOTONS

AUGER ELECTRONS

γ RAYS

INCIDENT BEAM ——————————→ SAMPLE HEATING

BREMSSTRAHLUNG

SPECIMEN

ELASTIC SCATTERING

CHARACTERISTIC X-RAYS

NUCLEAR REACTION PRODUCTS

FIG. 1

M_1 ● E_0 → E ◉ M_2

$\pi - \theta$

$E' = KE$

M_1
●
E_f

DETECTOR

0 t X

Fig 2

BACKSCATTERING

E_{in}

FILM SUBSTRATE

θin

θout

KE_{in}

E_f

DETECTOR

$E_\uparrow$

$KE_\uparrow$

X

t

O

NUMBER COUNTS

ΔE

E_f KE_{in} E_{in}

E

Fig. 3

Fig 4

Fig.

Fig 6

E

1.92 MeV

$^{16}O+d$

P_1

P_0

1/2+ 0.8707 MeV

γ

^{17}O

Fig 7

Fig 8

d ON GaAs ANODIC OXIDE

$^{16}O(d,p_1)^{17}O$

$^{16}O(d,p_0)^{17}O$

$^{12}C(d,p_0)^{13}C$

COUNTS

E(MeV)

Fig 9

Fig 10

SUPERCONDUCTING SOLENOID

Glaser field $B = \dfrac{B_0}{1+\left(\frac{Z}{a}\right)^2}$; $a = 6.5$ cm

$\Delta = \left(\dfrac{B_{Glaser}-B_{SS}}{B_0}\right)$

$\Delta > 0$

$\Delta < 0$

> 0

(cm) →

$F_{\underset{<}{\cdot}}$ //

VERTICAL
VAN DE GRAAFF
ACCELERATOR

PIEZOELECTRIC
XY DRIVE

S_1 ─ ─ $\frac{1}{2}\Delta y$

$\frac{1}{2}\Delta y$

1mr

$Q_{1,2,3}$

3mr

30mr

μ-SLITS

DIVERGENCE
SLITS

SUPERCONDUCTING
SOLENOID

$\Delta y = 0.012" \longrightarrow \frac{\Delta E}{E} = 10^{-4}$

SOURCE

OBJECT

IMAGE

2.13m

0.66m

0.80m

0.34m

0.11m

$M_x = M_y = \frac{i}{0} = \frac{1}{10}$
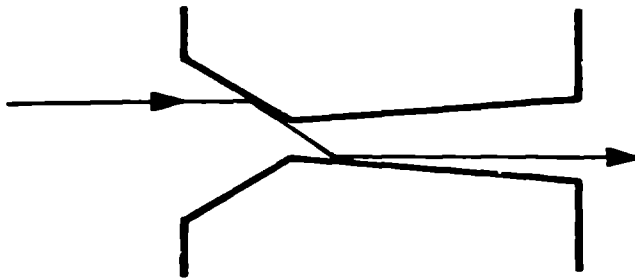
Fig 12

OBJECT SLITS

} WRONG DIRECTION AND WRONG
ENERGY FOR PROPER FOCUS

APPARENT EDGE THICKNESS t
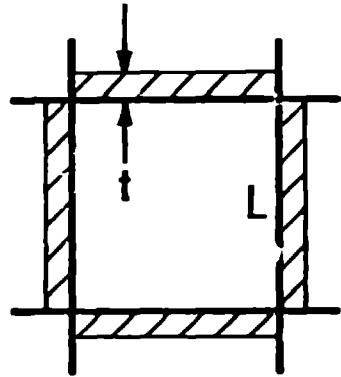
$$P/B \sim \frac{L^2}{4tL} \sim \frac{L}{t}$$

HEIDELBERG DESIGN

- DOUBLE SCATTERING

- HIGH Z FOR LARGE RMS
  SCATTERING THROUGH THE EDGE

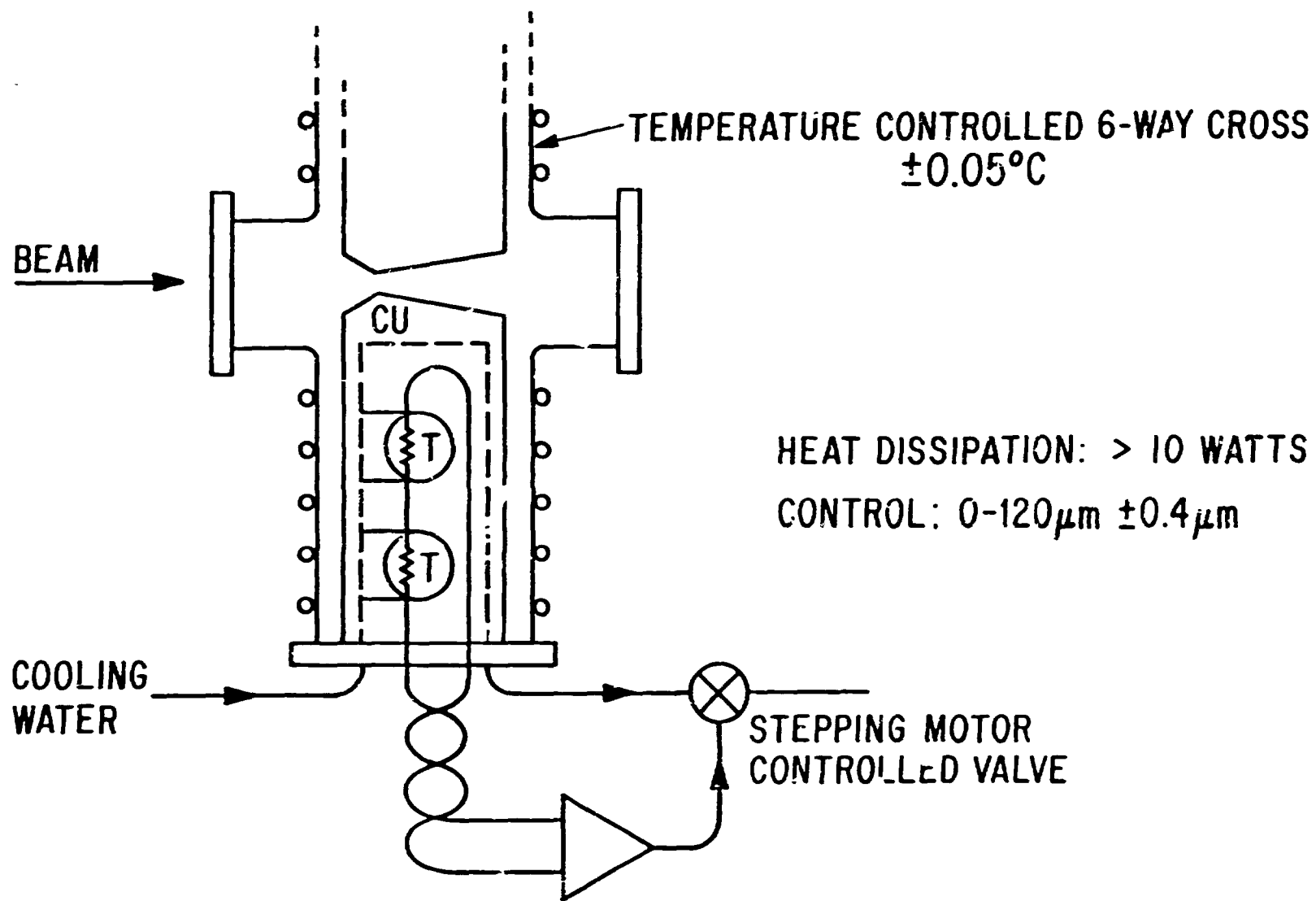- Au ON Cu MICROMACHINED
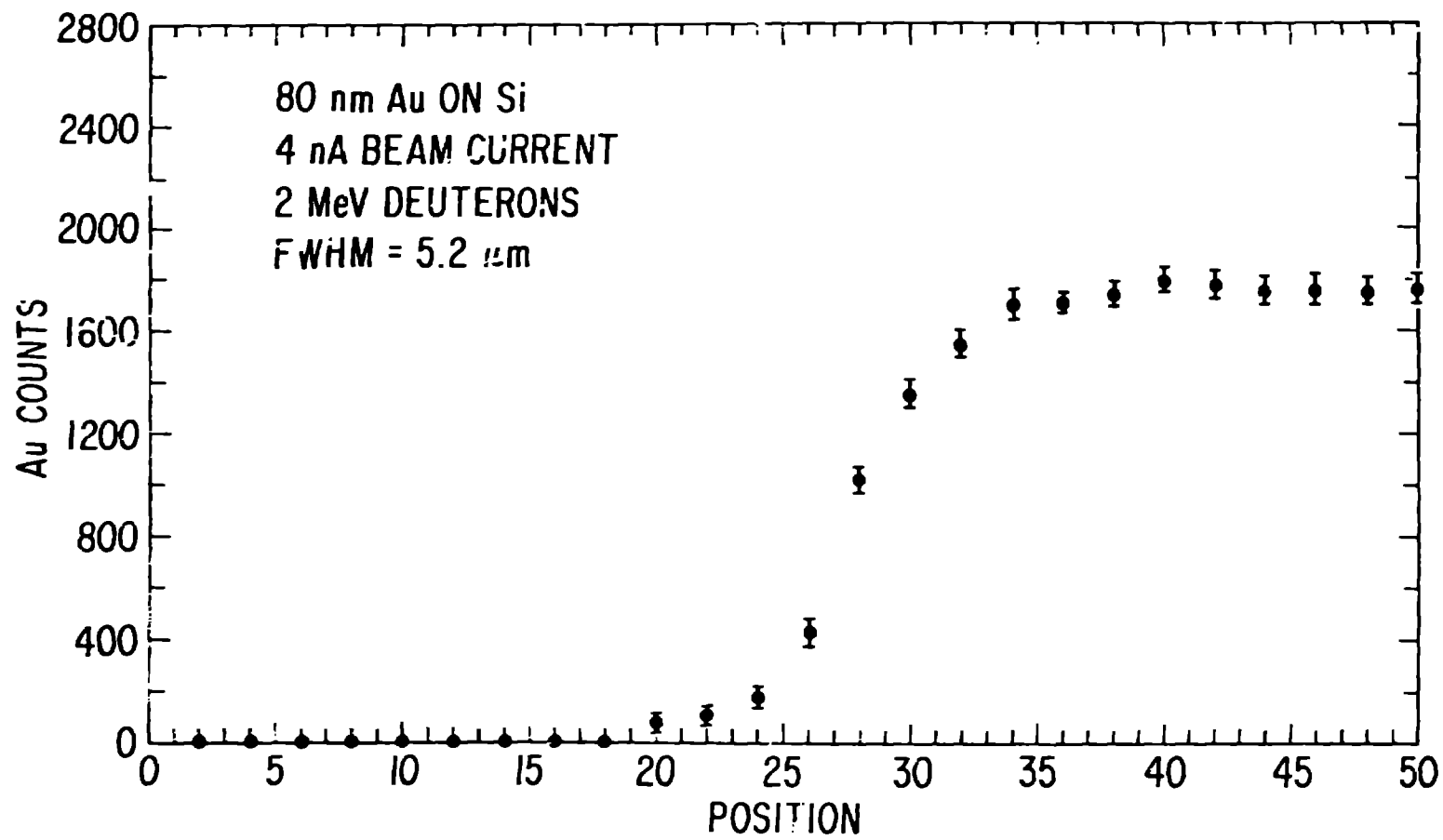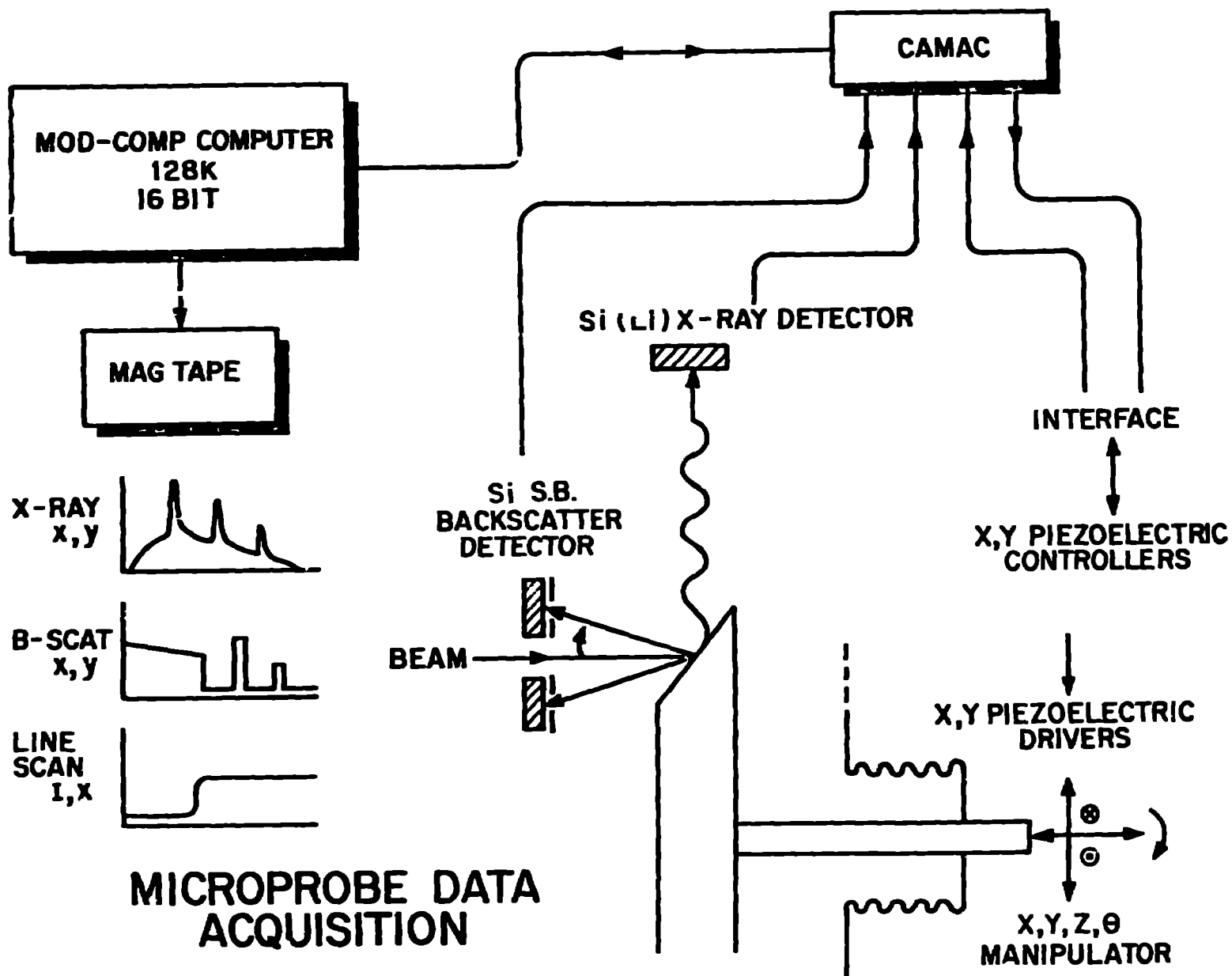
Fig 13

TEMPERATURE CONTROL OF MICRO-JAWS

TEMPERATURE CONTROLLED 6-WAY CROSS
±0.05°C

BEAM

CU

HEAT DISSIPATION: > 10 WATTS

CONTROL: $0-120\mu m \pm 0.4\mu m$

COOLING
WATER

STEPPING MOTOR
CONTROLLED VALVE

Fig 14

Fig 15

CAMAC

MOD-COMP COMPUTER
128K
16 BIT

MAG TAPE

Si (LI) X-RAY DETECTOR

INTERFACE

X-RAY
x,y

B-SCAT
x,y

LINE
SCAN
I,x

Si S.B.
BACKSCATTER
DETECTOR

BEAM

X,Y PIEZOELECTRIC
CONTROLLERS

X,Y PIEZOELECTRIC
DRIVERS

MICROPROBE DATA
ACQUISITION

X,Y,Z,θ
MANIPULATOR

Fig 16